



Polarization Entangled State Measurement on a Chip

Linda Sansoni,¹ Fabio Sciarrino,^{1,2} Giuseppe Vallone,^{3,1} Paolo Mataloni,^{1,2} Andrea Crespi,^{4,5}
Roberta Ramponi,^{4,5} and Roberto Osellame^{4,5}

¹Dipartimento di Fisica, Sapienza Università di Roma, I-00185 Roma, Italy

²Istituto Nazionale di Ottica, Consiglio Nazionale delle Ricerche (INO-CNR), Largo Enrico Fermi 6, I-50125 Firenze, Italy

³Museo Storico della Fisica e Centro Studi e Ricerche Enrico Fermi, Via Panisperna 89/A,
Compendio del Viminale, I-00184 Roma, Italy

⁴Istituto di Fotonica e Nanotecnologie, Consiglio Nazionale delle Ricerche (IFN-CNR),
Piazza Leonardo da Vinci, 32, I-20133 Milano, Italy

⁵Dipartimento di Fisica, Politecnico di Milano, Piazza Leonardo da Vinci, 32, I-20133 Milano, Italy
(Received 18 June 2010; published 10 November 2010)

The emerging strategy to overcome the limitations of bulk quantum optics consists of taking advantage of the robustness and compactness achievable by integrated waveguide technology. Here we report the realization of a directional coupler, fabricated by femtosecond laser waveguide writing, acting as an integrated beam splitter able to support polarization-encoded qubits. This maskless and single step technique allows us to realize circular transverse waveguide profiles which are able to support the propagation of Gaussian modes with any polarization state. Using this device, we demonstrate quantum interference with polarization-entangled states and singlet state projection.

DOI: 10.1103/PhysRevLett.105.200503

PACS numbers: 03.67.Bg, 03.67.Lx, 42.50.Dv, 42.79.Gn

Photons are a natural candidate for quantum information (QI) transmission [1,2], quantum computing [3,4], optical quantum sensing, and metrology [5]. However, the current optical technology does not allow the transition to ultimate applications because of many practical limitations. Complex quantum optical schemes, realized in bulk optics, suffer from severe drawbacks, as far as stability, precision, and physical size are concerned. Indeed, it is a difficult task to build advanced interferometric structures using bulk-optical components with the stability and optical phase control accuracy necessary to reach the sensitivity allowed by quantum mechanics. Furthermore, it is very difficult to reach this goal outside environments with controlled temperature and vibrations, and this makes applications outside the laboratory hard to achieve.

The present approach to beat these limitations is to adopt miniaturized optical waveguide devices. Very recently it was reported [6,7] that silica waveguide circuits integrated onto silicon chips can be successfully used to realize key components of quantum photonic devices. Inherently stable interferometers were shown to demonstrate phase stability, not only of single path-encoded qubits, but also of a two-photon entangled Fock state. On this basis, miniaturized integrated quantum circuits were realized to implement the first integrated linear optical control-NOT gate, achieving a fidelity very close to the theoretical value [6]. More recently, novel components for adaptive quantum circuits have also been demonstrated [8]. These experiments show robust and accurate phase control in integrated, path-encoded waveguide systems. Similar results have been obtained in UV laser written optical circuits

fabricated in a suitable stack of doped silica layers on a silicon substrate [9].

All the experiments performed so far with integrated quantum circuits are based only on path-encoded qubits with a given polarization state of the photons. On the other hand, many QI processes and sources of entangled photon states are based on the polarization degree of freedom [4]. One important example is given by states built on many photons [10] and/or many qubits, and by several schemes of one-way optical quantum computing [11]. Hence it is of essential interest to include the use of photon polarization in quantum circuits by fabricating integrated polarization independent devices, i.e., ones that are able to efficiently guide and manipulate photons in any polarization state.

It has to be noticed that the above-mentioned silica-on-silicon and UV written integrated waveguides suffer from intrinsic birefringence (usually reported on the order of 4×10^{-4} [12,13]). In fact, these waveguides are fabricated in a doped silica multilayer structure on a silicon substrate, and this causes material stress due to lattice mismatches between the different layers. Techniques for reducing this stress and the induced birefringence have been proposed, but they pose serious difficulties in terms of fabrication complexity and reproducibility [14]. Such birefringence causes polarization-mode dispersion and results in polarization dependent behavior of the integrated devices, which removes indistinguishability between the two polarizations. Moreover, propagation in birefringent structures can cause decoherence of large-bandwidth (short coherence time) photons typically generated in parametric down-conversion experiments. As a consequence, the

techniques already employed for producing path-encoded quantum circuits are not appropriate for processing polarization-encoded qubits in integrated devices.

In the present paper we show how to guide and manipulate photons in any polarization state by adopting a recently introduced technique, based on the use of ultrashort laser pulses, for direct writing of photonic structures in a bulk glass [15,16]. Precisely, here, for the first time, we demonstrate the maintenance of polarization entanglement and Bell-state analysis in an integrated symmetric (50/50) beam splitter, opening the way for the use of polarization entanglement in integrated circuits for QI processes.

Direct fabrication of buried waveguides in glass is obtained by femtosecond laser micromachining. Femtosecond infrared pulses, focused into the substrate using a microscope objective, induce nonlinear absorption phenomena based on multiphoton and avalanche ionization. These processes lead to plasma formation and energy absorption in a small region confined around the focus, causing a permanent and localized modification of the bulk material. Adjusting the processing parameters, a smooth refractive index increase can be obtained, and light-guiding structures are produced by translating the substrate with respect to the laser beam. Microscopic mechanisms leading to an increase of the refractive index are complex and include densification, structural modification, color centers formation, thermal diffusion, and accumulation. They concur in different ways depending on the specific material and fabrication parameter combination, i.e., wavelength, duration and energy of the laser pulses, repetition rate, objective numerical aperture, and translation speed [17].

The ultrafast laser writing approach has several advantages: (i) it is a maskless technique, thus particularly suited for rapid prototyping of devices; (ii) it can easily fabricate buried optical waveguides in a single step; (iii) it can produce optical circuits with three-dimensional layouts; and (iv) it can provide waveguides with a circular transverse profile [18] that can support the propagation of Gaussian modes with any polarization state, with very low waveguide form birefringence. Ultrafast laser written (ULW) waveguides in fused silica substrates have recently been employed for quantum optics experiments, still with path-encoded qubits [19]. However, it is known that ULW waveguides in fused silica are affected by material birefringence [20] (in particular, when high refractive index changes are required, as in the case of curved waveguides) due to the formation of self-aligned nanogratings in the material during the irradiation process [21]. Moreover, fabricating waveguides in fused silica is a rather slow process (on the order of 10–100 $\mu\text{m}/\text{s}$) [22]. For these reasons we chose to employ a borosilicate glass (EAGLE2000, Corning) as a substrate, where the formation of nanogratings has never been observed [22]. In addition, high repetition rate laser pulses induce isotropic thermal diffusion and melting of the material around the focal point [23], providing an almost circular waveguide cross section without the need for any shaping of the

writing laser beam. Very low-loss waveguides are obtained with translation speeds as high as 1–5 cm/sec, allowing extremely short processing times [24]. This represents an advantage for the realization of complex photonic circuits.

At wavelengths around 800 nm the waveguides support a single Gaussian mode of circular profile with 8 μm diameter at $1/e^2$ (see the near-field intensity profile of the guided modes in the lower inset of Fig. 1), allowing an 85% overlap integral with the measured mode of the fiber used (Thorlabs SM800-5.6-125) and leading to 0.7 dB estimated coupling losses. Measured propagation losses are 0.5 dB/cm, and using a curvature radius of 30 mm, additional bending losses are lower than 0.3 dB/cm. The birefringence of the ULW waveguides has also been characterized [24], providing a value $B = 7 \times 10^{-5}$, thus about 1 order of magnitude lower than silica-on-silicon waveguides.

Ultrafast laser written beam splitters (ULWBS) were fabricated with the directional coupler geometry, as shown in Fig. 1. Straight segments and circular arcs of 30 mm radius were employed for an overall device length of 24 mm. Waveguides start with a relative distance of 250 μm , and in the interaction region, they get as close as 7 μm (see the upper inset in Fig. 1). This distance is the smallest one avoiding overlap between the two waveguides. This choice was made to minimize the sensitivity to fabrication imperfections and to obtain the shortest possible interaction length, given that future quantum optic devices will require several cascaded components integrated in the same chip. In order to optimize the length L of the central straight segments, several directional couplers have been fabricated varying such length ($L = 0$ –1000 μm), and the corresponding splitting ratios were measured. $L = 0 \mu\text{m}$ is the shortest length yielding a splitting ratio of about 50% (see the ULWBS output modes in the lower inset in Fig. 1) at an 806 nm wavelength.

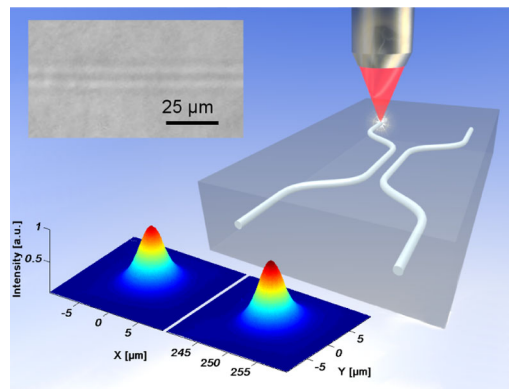


FIG. 1 (color online). Schematic of the femtosecond-laser-written directional coupler in the bulk of a borosilicate glass. The upper inset shows a microscope image of the two waveguides in the coupling region. The lower inset shows the near-field intensity profile of the output guided modes of the directional coupler when launching light in a single input; the symmetric Gaussian shape and the balanced splitting in the two arms can be appreciated.

Indeed, the possibility of achieving a 50% splitting with no straight segments is due to the coupling between the modes already occurring in the curved parts of the two approaching or departing waveguides. The reflectivity of the ULWBS for the horizontal and vertical polarizations was measured with a tunable laser operating at 806 nm. The measured unbalance between the two reflectivities $R_H = (49.2 \pm 0.2)\%$ and $R_V = (58.1 \pm 0.2)\%$ is attributed to a residual ellipticity in the waveguide profile, notwithstanding the thermal mechanism of the waveguide formation. Work is in progress to further optimize the waveguide cross section with the astigmatic beam shaping technique [18].

We demonstrated the ability of the chip to preserve any incoming polarization state by measuring the polarization degree (G) and obtaining $G \geq 99.8\%$.

The suitability of the ULWBS to handle polarization-encoded qubits was demonstrated by manipulating polarization-entangled states. The four Bell states $|\psi^+\rangle = \frac{1}{\sqrt{2}}(|H\rangle_A|V\rangle_B \pm |V\rangle_A|H\rangle_B)$, $|\phi^+\rangle = \frac{1}{\sqrt{2}}(|H\rangle_A|H\rangle_B \pm |V\rangle_A|V\rangle_B)$ represent an entangled basis for the four-dimensional Hilbert space describing the polarization of two photons. They can be grouped into the singlet state $|\psi^-\rangle$ that generates the antisymmetric subspace, and the triplet states $\{|\psi^+\rangle, |\phi^+\rangle, |\phi^-\rangle\}$ that generate the symmetric subspace, where the symmetry refers to the exchange of the two photons [25]. The beam splitter can be used to discriminate between the symmetric and antisymmetric subspaces. Indeed, if two photons in the singlet state $|\psi^-\rangle$ impinge simultaneously on a 50/50 beam splitter, they will always emerge on different outputs of the beam splitter due to quantum interference. Conversely, for any state orthogonal to $|\psi^-\rangle$ (thus belonging to the symmetric subspace) the two photons will be found in the same output mode.

The setup adopted in the experiment is shown in Fig. 2. To observe the appearance of the bosonic coalescence for input symmetric states, we varied the relative delay between the two photons and hence their corresponding temporal superposition on the ULWBS [26]. We first tested the Hong-Ou-Mandel [26] effect with separable states, by placing two polarizing beam splitters (PBS) in the k_A and k_B modes (see Fig. 2). We report in Fig. 3(a) the coincidence counts as a function of the shift Δx in the delay line for two photons in the input state $|HH\rangle$. The experimental visibility is defined as $V_{\text{exp}} = |\frac{\mathcal{C}_0 - \mathcal{C}_{\text{int}}}{\mathcal{C}_0}|$, where \mathcal{C}_0 and \mathcal{C}_{int} correspond, respectively, to the coincidence rate outside interference (i.e. with Δx larger than the photon coherence length) and inside interference ($\Delta x = 0$). The measured visibility is $V = 0.937 \pm 0.009$. We performed the same measurement with the input states $|VV\rangle$ and $|++\rangle$, obtaining $V = 0.926 \pm 0.012$ and $V = 0.954 \pm 0.011$, respectively. We also tested the interference with entangled states. When the photons arrive simultaneously on the ULWBS ($\Delta x = 0$ in the figure), we measured for the triplet (singlet) a dip (peak) in the coincidence counts, as expected [see Fig. 3(b)]. The measured visibilities are $V_{|\text{singlet}\rangle} = 0.930 \pm 0.005$ and $V_{|\text{triplet}\rangle} = 0.929 \pm 0.005$.

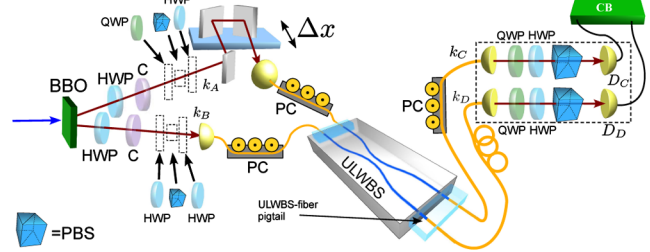


FIG. 2 (color online). Setup for the quantum optics experiments showing the source of polarization-entangled photons, the ULWBS, and the detection system. The polarizing beam splitter, HWP, and QWP were optionally inserted in path k_A and k_B depending on the different input states. A delay line Δx in the k_A arm enabled a temporal delay variation between the two input photons. The components shown in the dashed box were inserted only during the tomography measurement of the filtered state. C is for crystal compensators, and PC is for polarization controllers.

We attribute the slight discrepancy observed between the theoretical [27] and experimental values to a partial spectral distinguishability between the photons on modes k_A and k_B ; this could be reduced by using narrower bandwidth detection filters.

Let us now analyze the behavior of the different entangled states. The temporal delay was set at $\Delta x = 0$, and the source was tuned to generate the entangled state $|\psi^+\rangle$. By inserting on mode k_B a half wave plate (HWP) with the optical axis oriented at an angle θ with respect to the vertical direction, the following states are generated: $- \cos 2\theta |\psi^-\rangle + \sin 2\theta |\phi^+\rangle$. In this case, the expected coincidence rate between detectors D_C and D_D after the beam splitter is $\mathcal{N}_0[1 + \tilde{V} \cos 4\theta]$, where \mathcal{N}_0 is the average coincidence rate, and the expected visibility with

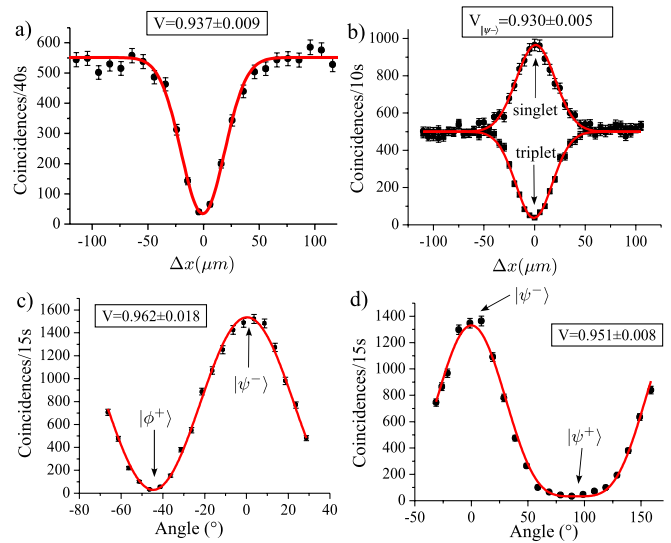


FIG. 3 (color online). (a) Hong-Ou-Mandel dip with input state $|HH\rangle$. (b) The peak or dip corresponding to the singlet or triplet input state. (c) Fringe pattern obtained by rotating the HWP on mode k_B . (d) Fringe pattern obtained by rotating the QWP on mode k_A . All curves represent experimental fits.

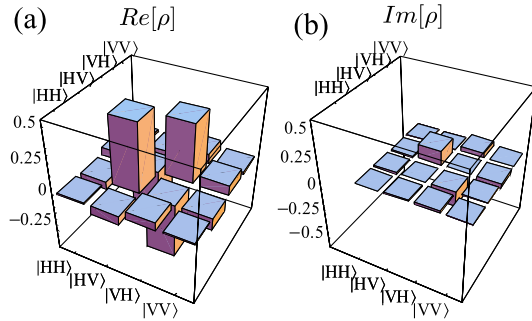


FIG. 4 (color online). Quantum state tomography of a filtered singlet state on the two output modes k_C and k_D . Panels (a) and (b) show the real and imaginary parts, respectively, of the experimental density matrix of the filtered state.

the given R_H and R_V is $\tilde{V} = 0.973$. The experimental results are shown in Fig. 3(c), yielding a visibility $V = 0.962 \pm 0.018$.

When the source is tuned to generate the entangled state $|\psi^i\rangle = \frac{1}{\sqrt{2}}(|H\rangle_A|V\rangle_B - i|V\rangle_A|H\rangle_B)$, by using a quarter wave plate (QWP) rotated at θ' on mode k_A , the state is found to be $\cos^2\theta'|\psi^-\rangle - i\sin^2\theta'|\psi^+\rangle + \frac{e^{-i(\pi/4)}}{\sqrt{2}}\sin2\theta'|\phi^i\rangle$ with $|\phi^i\rangle = \frac{1}{\sqrt{2}}(|HH\rangle + i|VV\rangle)$. For the sake of simplicity, by assuming polarization independent reflectivity, the coincidence rate expected with a beam splitter with reflectivity R is $\mathcal{N}_0[1 - V_{\text{theo}} + 2V_{\text{theo}}\cos^4\theta']$, where $V_{\text{theo}} = 2(1 - R)R/(2R^2 - 2R + 1)$. By taking $R = (R_H + R_V)/2$ we expect $V_{\text{theo}} = 0.987$. The theoretical behavior was verified in the experiment. The corresponding fringe pattern, with visibility $V = 0.951 \pm 0.008$, is shown in Fig. 3(d). These results demonstrate the high overlap between the interfering modes k_A and k_B and show that ULWBS may be used as an appropriate tool for the manipulation of a polarization-encoded qubit.

As a final experimental characterization we adopted the ULWBS to carry out the projection on a singlet subspace. We injected into the ULWBS the separable state $|H\rangle_A \otimes |V\rangle_B$ and analyzed the output state when two photons emerge on the two modes k_C and k_D ; the expected state reads $|\psi^-\rangle_{CD}$. We performed the quantum state tomography [28] of the output state conditioned to the detection of the two photons in different outputs. In this case two standard polarization analysis setups were adopted after the ULWBS (see the dashed box in Fig. 2). The experimental density matrix ρ_{CD} shown in Fig. 4 exhibits a low entropy ($S_L = 0.071 \pm 0.018$), a high concurrence ($C = 0.941 \pm 0.015$), and a high fidelity with the singlet state ($F = 0.929 \pm 0.007$). We observe that the present scheme achieves *a posteriori* singlet component filtration, i.e., conditioned to the detection of one photon per output mode. Recently, a heralded entanglement filter, based on two auxiliary photons and an interferometric scheme, was reported by adopting a bulk-optical scheme in Ref. [29].

In summary, we reported on the realization and quantum optical characterization of a femtosecond-laser-written

directional coupler, acting as an integrated beam splitter. The experimental results demonstrate the suitability of this method to manipulate qubits encoded in the polarization of photon states. In order to achieve a complete handling of the polarization degree of freedom, the next step will consist in the realization of integrated tunable wave plates and polarizing beam splitters. By combining these tools with integrated sources of photon pairs and, possibly, with integrated detectors, the realization of a pocket quantum optics lab, available for optical quantum sensing, computing, and metrology, may become a reality in the near future.

This work was supported by the FARI project, Finanziamento Ateneo 2009 of Sapienza, FIRB-Futuro in Ricerca HYTEQ, and Finanziamento Ateneo 2009 of Politecnico di Milano.

- [1] N. Gisin *et al.*, Rev. Mod. Phys. **74**, 145 (2002).
- [2] L.-M. Duan *et al.*, Nature (London) **414**, 413 (2001).
- [3] T. D. Ladd *et al.*, Nature (London) **464**, 45 (2010).
- [4] P. Kok *et al.*, Rev. Mod. Phys. **79**, 135 (2007).
- [5] J. Dowling, Contemp. Phys. **49**, 125 (2008).
- [6] A. Politi *et al.*, Science **320**, 646 (2008).
- [7] A. Politi, J. C. F. Matthews, and J. L. O'Brien, Science **325**, 1221 (2009).
- [8] J. Matthews *et al.*, Nat. Photon. **3**, 346 (2009).
- [9] B. J. Smith *et al.*, Opt. Express **17**, 13516 (2009).
- [10] R. Krischek *et al.*, Nat. Photon. **4**, 170 (2010).
- [11] P. Walther *et al.*, Nature (London) **434**, 169 (2005).
- [12] M. Kawachi, Opt. Quantum Electron. **22**, 391 (1990).
- [13] D. Johlen *et al.*, J. Lightwave Technol. **18**, 185 (2000).
- [14] Y. Inoue *et al.*, J. Lightwave Technol. **15**, 1947 (1997).
- [15] R. R. Gattass and E. Mazur, Nat. Photon. **2**, 219 (2008).
- [16] G. Della Valle, R. Osellame, and P. Laporta, J. Opt. A **11**, 013001 (2009).
- [17] R. Osellame *et al.*, IEEE J. Sel. Top. Quantum Electron. **12**, 277 (2006).
- [18] R. Osellame *et al.*, J. Opt. Soc. Am. B **20**, 1559 (2003).
- [19] G. D. Marshall *et al.*, Opt. Express **17**, 12546 (2009).
- [20] G. Cheng *et al.*, Opt. Express **17**, 9515 (2009).
- [21] Y. Shimotsuma *et al.*, Phys. Rev. Lett. **91**, 247405 (2003).
- [22] M. Ams *et al.*, IEEE J. Sel. Top. Quantum Electron. **14**, 1370 (2008).
- [23] S. M. Eaton *et al.*, Opt. Express **16**, 9443 (2008).
- [24] See supplementary material at <http://link.aps.org/supplemental/10.1103/PhysRevLett.105.200503> for more details about the ULW technique and the experimental methods.
- [25] K. Mattle *et al.*, Phys. Rev. Lett. **76**, 4656 (1996).
- [26] C. K. Hong, Z. Y. Ou, and L. Mandel, Phys. Rev. Lett. **59**, 2044 (1987).
- [27] Since our ULWBS has different transmission (T) and reflection (R) coefficients for the H and V polarizations, the maximum expected visibilities are $V_\psi = 2\frac{\sqrt{T_H T_V R_H R_V}}{T_H T_V + R_H R_V} \simeq 0.989$ for $|\psi^\pm\rangle$ and $V_\phi = 2\frac{T_H R_H + T_V R_V}{T_H^2 + R_H^2 + T_V^2 + R_V^2} \simeq 0.974$ for $|\phi^\pm\rangle$.
- [28] D. F. V. James *et al.*, Phys. Rev. A **64**, 052312 (2001).
- [29] R. Okamoto *et al.*, Science **323**, 483 (2009).